Journal of Visualization, Vol. 1, No. 3 (1999) 291-301

Three-dimensional Bubbly Flow Measurement Using PIV

Hassan, Y. A.*, Schmidl, W. D.* and Ortiz-Villafuerte, J.*

* Department of Nuclear Engineering, Texas A&M University, College Station, Texas 77843-3133, USA.

Received 1 May 1998.
Revised 12 November 1998.

***Abstract*:** The experimental flow visualization tool, Particle Image Velocimetry (PIV), is being extended to determine the velocity fields in three-dimensional, two-phase fluid flows. In the past few years, the technique has attracted quite a lot of interest. PIV enables fluid velocities across a region of a flow to be measured at a single instant in time in the whole volume (global) of interest. This instantaneous velocity profile of a given flow field is determined by digitally recording particle (microspheres or bubbles) images within the flow over multiple successive video frames and then conducting flow pattern identification and analysis of the data. This paper presents instantaneous velocity measurements in various three-dimensional, bubbly two-phase flow situations. This information is useful for developing or improving existing computer constitutive models that simulate this type of flow field. It is also useful for understanding the detailed structure of two-phase flows.

***Keywords*:** three-dimensional measurement, particle image velocimetry, bubbly flow, conditional sampling, Reynolds stress.

1. Introduction

In two-phase flow studies, there is a major shift of research focus on the two-phase patterns (behavior) from macroscale to microscale structures, which presents not only new challenges but also new opportunities to achieve a better understanding and control of the physical phenomenon.

Particle Image Velocimetry (PIV) is a non-intrusive measurement technique, which can be used to study the structure of various fluid flows (Adrian,1991; Hassan et al.,1992a, 1992b; Yamamoto et al.,1995a). PIV is used to measure the time varying full field velocity data of a particle-seeded flow field within either a two-dimensional plane or three-dimensional volume. PIV is a very efficient measurement technique since it can obtain both qualitative and quantitative spatial information about the flow field being studied at one instant. This information can be further processed into information such as vorticity, pathlines, Reynolds stresses and kinetic turbulent energy, etc. Other flow measurement techniques (Laser Doppler Velocimetry, Hot Wire Anemometry, etc.) only provide temporal quantitative information at a single point.

PIV can be used to study turbulence structures if a sufficient amount of data can be acquired and analyzed, and it can also be extended to study two-phase flows if both phases can be distinguished. Some of the more recent works include Hilgers and Merzkirch (1992), Kasagi and Nishino (1991), Moursali et al. (1995), Murai and Matsumoto (1995), Oakley et al. (1995), Sridhar and Katz (1995), Yamamoto et al. (1995a), among others.

PIV relies on fast and accurate methods to track instantaneously numerous particles suspended in the flow. These micron size seed particles possess certain physical properties, which allow them to accurately follow the flow pathlines and respond to accelerations in the flow. The second phase can be bubbles with various diameters in continuous liquid phase or liquid droplets in continuous gas phase. In addition to the velocity fields, optical

imaging techniques are also capable of providing information about the concentration and size of the suspended phase and their distribution in space. The flow field for each phase can be independently determined since both phases can be distinguished on the images captured by the CCD cameras. The differentiation of the phases can be made by a comparison of their physical size on the images. Another way to distinguish each phase is by using fluorescent particles which absorb the incident light, and emit light with a different frequency (Philip et al., 1994; Hilgers and Merzkirch, 1992). In these situations, a camera with a filter and another camera without a filter are used. The camera with the filter will capture the fluorescent particles (one of the phases), while the other camera will capture both phases. The second-phase flow field is then determined by subtracting the filtered image from the unfiltered image.

A crucial element of the data processing is the particle tracking. Since a large quantity of data needs to be analyzed, the tracking process must be fast and reliable. Several tracking techniques have been developed and extended for three-dimensional measurements (Nishino et al.,1989; Reese et al.,1995; Trigui et al.,1992; Yamamoto et al. 1995a). Some of these routines are cross correlation methods (Hassan et al.,1992a ; Yamamoto et al.,1995b), spring model methods (Okamoto et al.,1995), neural network tracking schemes (Cenedese,1992; Grant et al.,1995; Hassan et al.,1997), and genetic algorithm techniques.

2. Experimental Setup

The flow structure around bubbles rising in a pipe filled with water was studied in three-dimensions. The velocity of the rising bubble and the velocity field of the surrounding water were measured. The turbulence intensities, Reynolds stresses, turbulent kinetic energy were inferred from the experimental data. Finally, the behavior of the turbulent kinetic energy within the measurement zone due to a rising bubble was delineated.

A test facility was constructed to conduct experiments on the interaction between a rising air bubble and surrounding fluid in a pipe flow. The facility setup consisted of a vertical clear glass pipe, a pump, and a water filter. The size of the pipe is 1.1×10^{-2} m inside diameter, and 1.5×10^{-2} m outside diameter. A five micron water filter was used to filter out any contaminants prior to the tracer particles being added to the water and the experiment being conducted.

The flow was seeded with small polystyrene tracer particles. The density of these particles is 1050 kg/m^3. Their diameter is 40×10^{-6} m. The particle diameter needs to be small enough to effectively follow the flow, however, it also needs to be large enough to reflect enough light that their image can be captured by the cameras.

The optical setup includes an Argon laser, an Acousto Optic Modulator (AOM or Bragg cell), mirrors, a beam splitter lens, and a multimode fiber with a fiber coupler as shown in Fig. 1. The light source is a 5 W Argon ion laser. It produces light at approximately 514 nm (which corresponds to green light). The laser beam passes through the AOM, which chops the beam as triggered by the computer. This allows the timing between the laser

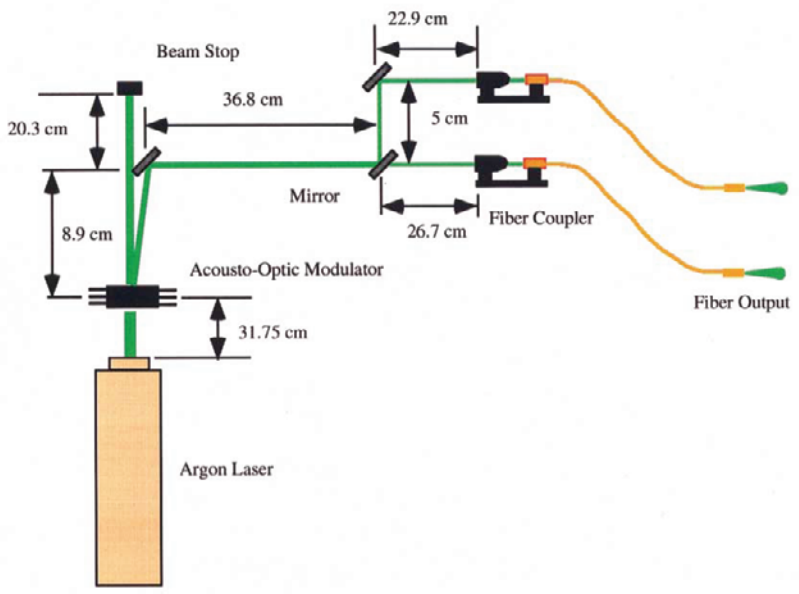

Fig. 1. Laser setup for obtaining two light beams.

and the computer to be controlled. The AOM consists of an optic medium coupled with an acoustic wave generator. When an acoustic wave is present in the optical medium, it creates a pressure wave in the medium in a sinusoidal shape. The refractive index of the medium is affected by the pressure wave and, as a consequence, a refractive index wave is generated in the optical medium that behaves like a sinusoidal grading. When the incident light from the laser passes through the grading it is diffracted into several orders. The first order is used to illuminate the viewing volume.

The computer imaging board is used to send a pulse signal to the acoustic wave generator of the AOM, to generate a pulse of light. The width of the light pulse is equal to the width of the pulse signal received by the acoustic wave generator. The interval between pulse signals controls the interval between light pulses. The acoustic wave generator sends the acoustic wave into the AOM's optic medium to generate the first order beam.

After the AOM, the first order beam is directed by a mirror to a beam splitter which separates the beam into two parts. Each part is directed to a separate fiber coupler. The beam then passes into a 400 $\times 10^{-6}$ m multimode fiber, which transmits the beam to the experimental test section.

The data acquisition system consists of four digital cameras, each equipped with a telephoto lens, a 2x range extender, a close-up lens, and a light intensifier system with a gain factor of 1:12000. The cameras have a resolution of 640 $\times$ 480 pixels when run in RS-170 frame interlace mode at 30 frames per second. By running the camera in field mode, the resolution is reduced to 640 $\times$ 240, however, the framing rate is increased to 60 frames per second. The cameras were run in field mode to take advantage of the higher framing rate. Since the camera image is two-dimensional, particle positions for two out of three coordinates may be easily calculated from one camera image, which is perpendicular to the test section wall. The other coordinate should be determined using information obtained from the other camera (Costes,1994). Since only two cameras are needed to determine the three-dimensional position of the particles, by using four cameras, two sets of coordinates are obtained for each instant in time. These two sets of data can be compared or combined later. This increases the probability of identifying the seeds. The facility setup and basic camera arrangement are illustrated in Fig. 2. Figure 3 shows the method that was used to find the three-dimensional position of the particles from two-cameras. From the image of the perpendicular camera to the test section, x and y coordinates are directly obtained.

As it can be seen in Fig. 2, the viewing volume was enclosed in a thin-wall, transparent, plexiglass-made box full with water. The refraction indices of the glass pipe, plexiglass box, and water are all between 1.3 and 1.5. This set up helped to reduce the refraction effect of the curved wall of the pipe, as was demonstrated during the calibration procedure. Moreover, camera calibration was performed *in situ*, under the same conditions in which the experimental measurements were carried out. In this way, the images of the calibration grid points have already incorporated the refraction effects.

Each set of two cameras was positioned such that the distance from the center of the pipe to each camera is

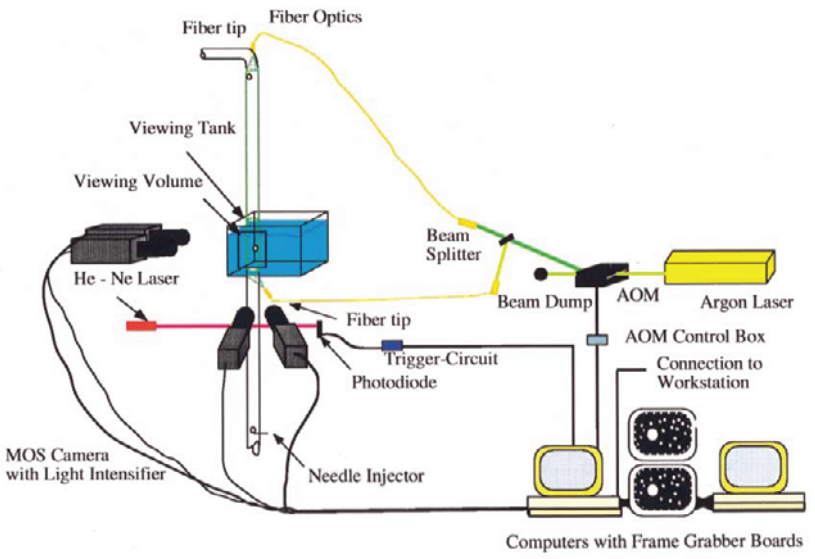

Fig. 2. Facility setup for the bubbly flow pipe experiment.

approximately the same. This allowed for having similar focal length and magnification factor on the cameras. In each set of cameras, one of the cameras was assumed to have its optical axis perpendicular to the plexiglass face, that is, the camera's image plane, the plexiglass box face, and the calibration grid are all parallel. Further, all 4 cameras were assumed to have the Y-direction image coordinates to be the same. Our calibration results proved that the camera positioning and all previous assumptions were effectively achieved.

The calibration grid was a matrix-like pattern of tiny white circular dots on a black background, printed out on a thin transparency. The camera calibration is done by moving the grid along two-perpendicular axes with a 3-way micro positioning stage. The accuracy of the micrometer is less than 0.01 mm. The grid is moved various known distances and the displacement of grid points are recorded.

The three-dimensional flow field is reconstructed by using a stereoscopic technique as shown in Fig.3. The data from the two-dimensional images are first tracked using an Adaptive Resonance Theory (ART-2) Neural Network technique which will be described briefly in the following section. The three-dimensional information is obtained from the two independent camera images from the displacement in corresponding vector positions between the two images. The relationship between the displacement in corresponding two-dimensional vector positions and the calculated three-dimensional vector position is obtained from the camera setup calibration. In other words, a function f relating the difference in the X-direction image coordinates between the perpendicular and its associated cameras is constructed from the calibration data. The accuracy of f will naturally depend on the calibration error.

The experimental data images are recorded at 60 frames per second. After acquiring the images, a displacement field in pixel values is obtained. By calibrating the pixels to spatial values, and knowing the time difference between successive exposures, the velocity field can be obtained. Figure 4 presents a two-dimensional binary overlay (a superposition of a number of frames on a single image) of the 8 frames from one camera when the bubble is present. This figure shows the Z-X plane captured by one camera. The other camera will capture a plane rotated ø degrees from the perpendicular view. By combining both images the three-dimensional flow field is reconstructed.

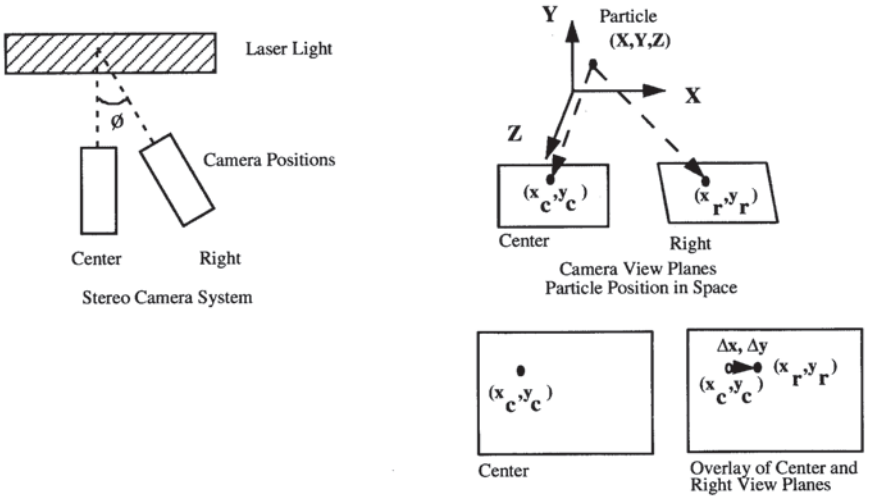

Fig. 3. Two-dimensional camera view planes for a particle at (X,Y, Z).

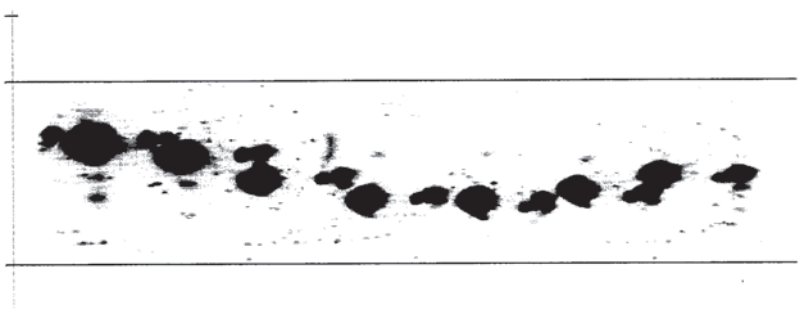

Fig. 4. Binary overlay of 8 frames.

3. Tracking Routine

The experimental particle data was first tracked two-dimensionally using an ART-2 Neural Network tracking algorithm. Four individual sequential frames were tracked, each iteration. This process was repeated throughout each set of 27 frames.

The transformation of the particle positions from the image plane into parameter space is depicted in Fig. 5. The black spot in Fig. 5(a) represents the particular particle, from the first frame, for which possible tracks are being assumed. The ellipse surrounding the black spot represents the search region. Particles from the next three frames, which fall in the search region, are included in the calculation.

The spatial relationship between these particles is converted into angular and intercept data, by the use of Hough Transform (Gonzalez et al.,1987). This step is shown also in Fig. 5(b). This data is then grouped into clusters, by use of the ART-2 neural network.

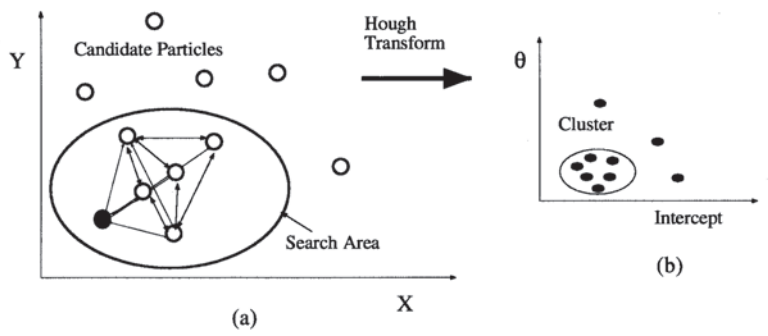

Fig. 5. Image plane and parameter space.

Figure 6 depicts the procedure by which individual candidate particles are processed into vectors. The Hough transform is used to identify the angular and intercept data between particles. These data are classified into clusters by using a decision system. The network identifies tight clusters. The clusters are then fed into a filtering routine, which selects the best possible vector based on how well its characteristics match the flow conditions. Details of this tracking routine and its performance can be obtained from Hassan et al. (1997).

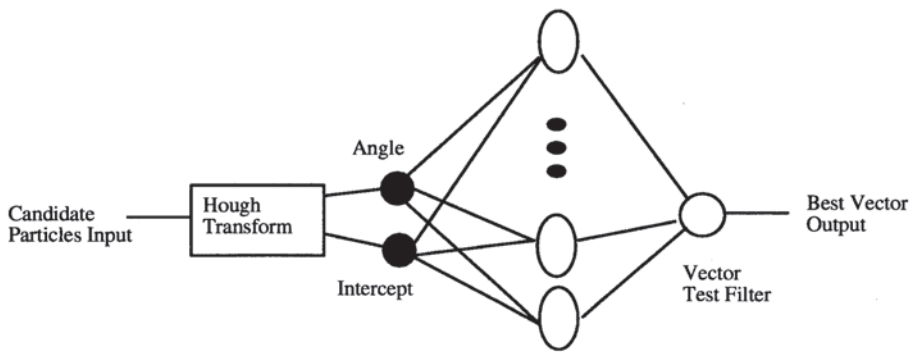

Fig. 6. System showing that the output of the hough transform (HT) is used directly as inputs to the NN and the vector test filter.

4. Error Estimation

The viewing section was 2.46 $\times 10^{-2}$ m high and 1.86 $\times 10^{-2}$ m wide. The spatial resolution for the 640 $\times$240 pixel resolution cameras was determined to be 7.80 $\times 10^{-5}$ m/pixel in the radial direction and 3.80 $\times 10^{-5}$ m/pixel in the axial direction. The resolution error was then 7 % in the radial direction and 3.8% in the axial direction.

The Stokes number, St, gives an estimate of the response of the tracer particles to changes in the fluid

motion. This is given by,

$$St = \frac{\tau_p}{\tau_f} \tag{1}$$

where τ_p is the relaxation time of the particle, and τ_f is the characteristic time of the fluid. The relaxation time, τ_p, can be calculated from,

$$\tau_p = \frac{(2\rho_p + \rho_f)\, d_p^2}{36\mu_f} \tag{2}$$

and

$$\tau_f = \frac{D}{U} \tag{3}$$

where, D is the characteristic length, and U is the bulk velocity. For our measurements, $\tau_p = 140 \times 10^{-6}$ s. For the limiting case of τ_f, we consider the highest velocity achievable by the fluid, which is that of the rising bubble, 1.76×10^{-1} m/s. Then, for an equivalent diameter of 3.6 $\times 10^{-3}$ m, $\tau_f = 0.02$ s. This gives a Stokes number of $St = 6.84 \times 10^{-3}$ s, which is much less than 1. Therefore, the tracer particles accurately reflected fluid motion changes.

The accuracy of the measurements can be computed from (Adrian, 1986)

$$\sigma_U = \frac{\sigma_{\Delta x} + U\sigma_{\Delta t}}{\Delta_t} \tag{4}$$

where $\sigma_{\Delta x}$ is proportional to the error in locating the centers of the particle images, and it depends on camera and optical parameters as well. $\sigma_{\Delta t}$ is the uncertainty in the laser pulse separation. Δt is the time difference between laser pulses.

In our measurements, $\sigma_{\Delta x}$ was computed to be 7.12 μm. Δt was 16.6 ms, and the uncertainty $\sigma_{\Delta t}$ was measured, with an oscilloscope, to be 67 μs.

When particle tracking is to be performed, one of the input parameters is the maximum velocity to be followed. In our case, we set this limit to 25 $\times 10^{-3}$ m/s, which is a little higher than the maximum axial velocity of the liquid (22 $\times 10^{-3}$ m/s) in the second measurement, flowing under laminar flow conditions. The uncertainty for this maximum velocity was determined, from equation 4, to be 2 %.

For the cases of the radial and angular velocities, the reduced resolution affects the term $\sigma_{\Delta x}$. Since the spatial resolution in the y-direction is reduced by a half, the uncertainty in determining the centroid of the spot images doubles. Then, using the maximum axial velocity, the error in the radial and angular velocities was computed to be 3.9 %. Further, for these two components of the velocity vector, the error in determining the third dimension has to also be included in the error estimation. It was found that the function f had an uncertainty of ±0.035 mm, which corresponds to an 8.4 % error with respect to the maximum axial velocity. Then the total error in the angular and radial velocities was 9.26 %.

The framing rate of 60 frames/s does not allow for capturing turbulent phenomena of a higher frequency. According to the Nyquist sampling criterion, only those turbulent phenomena created by the bubble's wake with a frequency lower than 30Hz could be acquired in this experiment.

5. Results

In this study, an investigation of the three-dimensional structure of the two phases in a concurrent, upward bubbly pipe flow was conducted by experimentally acquiring the instantaneous three-dimensional velocity field distributions of the two-phase flow with the three-dimensional Particle Image Velocimetry (PIV) technique. The first stage of this investigation is to study the interaction between a single rising bubble and the surrounding fluid in a pipe flow using a three-dimensional PIV measurement technique.

Three different measurements were performed. First, a measurement through the view volume when the fluid was at rest, and then a bubble was injected. Second, a single liquid-phase experiment with upward flow rate. Third, measurement was performed with a co-current upward bubbly flow with the same single phase flow rate as

in the second case. The injected water flow rate was 1.03 $\times 10^{-6}$ m^3/s (superficial liquid velocity, $jf = 1.09 \times 10^{-2}$ m/s), and the air flow rate was 6.17×10^{-9} m^3/s (air superficial velocity, $jg = 6.70 \times 10^{-6}$ m/s). The flow meter has an accuracy of $\pm 5\%$.

For the first measurement, the bubble rise velocity was determined to be 0.176 m/s. Its Reynolds number is 704.0, based on an equivalent bubble diameter of 4 $\times 10^{-3}$ m. In the second measurement, the liquid fluid velocity was 1.1×10^{-2} m/s. The Reynolds number was 121.0, based on the diameter of the tube. In the third measurement the bubble rise velocity was 0.169 m/s, and its equivalent diameter was measured to be ~3.6 $\times 10^{-3}$ m. The fluid velocity was also 1.1 $\times 10^{-2}$ m/s. The bubble Reynolds number was 632.0. Previous investigations (Chinnov and Volkov, 1991) show that the bubble shape is not exactly spherical, for the conditions mentioned above. The bubble equivalent diameter was determined by considering the injected air flow rate, and counting the number of bubbles generated for 60 seconds. Several pictures of the bubbles were also acquired at a fast shutter speed with a photographic camera equipped with telephoto and close-up lenses, to help determine the bubbles' dimensions and their shape. The pictures showed an ellipsoidal shape.

To determine the velocity distribution, the viewing volume was divided into small regions (segments) of size $r\Delta r\Delta z\Delta\theta$. In this measurement the length Δz and the azimuthal angle $\Delta\theta$ were fixed and equal to 2.46×10^{-2} m and 2π, respectively. The radius r was divided into 12 equal segments, each of width 4.58×10^{-4} m (~6 pixel).

Two different cases were considered to study the evolution of the fluid motion: when the bubble was present in the viewing volume, and after the bubble departed the viewing volume. For the bubble radial location in the pipe, the radius was divided into two regions. Region I closer to the wall, while Region II is closer to the pipe centerline, as delineated in Fig. 7. The fluid data was then conditionally sampled depending on the position of the bubble (Regions I or II, and if bubble is present or not in the view volume), to obtain the seeds velocities at the 12 radial locations. These conditions help to identify and quantify the turbulence generation, and to understand the transient behavior of the turbulence induced by a single bubble.

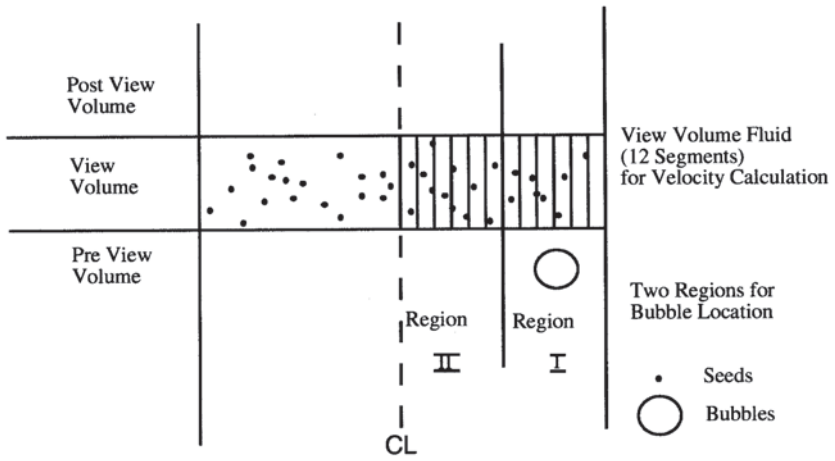

Fig. 7. Segmentation of the view volume.

The data points of the spatial distribution for different physical quantities of interest are determined by using an ensemble average in each region of the tube. The instantaneous velocity component i for a sample n is $u_i = u_i^n(r, \theta, z, t)$ where n is the number of the samples out of total N, and $i = r, \theta, z$ denotes the velocity components in r, θ, and z directions, respectively, at a position point $\boldsymbol{r}(r, \theta, z)$ in the view volume. The conditional sampling of the liquid mean velocity, $\overline{u_i}(r, \theta, z)$, can be evaluated from the instantaneous velocity components as follows :

$$\overline{u_i}(r, \theta, z) = \frac{1}{N}\left\{ \sum_{n=1}^{N} u_i^n(r, \theta, z) \middle| \boldsymbol{r}_b(r_b, \theta_b, z_b) \right\} \tag{5}$$

where N is the total number of samples in each of the 12 radial divisions, for a specified bubble location $\boldsymbol{r}_b(r_b, \theta_b, z_b)$. As mentioned above, the bubble locations were divided into three axial and two radial zones. When the bubble was present, the averaging was performed over about 800 frames. There was an average of 550 vectors per radial division. The average calculation is based on the total number of vectors in the viewing volume divided by the number of regions. After the bubble had left, there was an average of 3500 vectors per region.

The fluctuating velocity component, $u_i'^n(r,\theta, z, t)$, value can be calculated from

$$u_i'^n(r, \theta, z, t) = u_1^n(r, \theta, z, t) - \overline{u_i}(r, \theta, z) \tag{6}$$

These calculations were performed by first acquiring many instantaneous quantitative three-dimensional velocity field distributions in the pipe flow, numerically averaging the data to find the mean velocity components for the water phase, as given by Eq.(1). A similar equation as Eq.(1) can be employed to estimate the average velocity of the gas phase. The mean velocity value was subtracted from the instantaneous velocity to obtain the velocity fluctuation values as obtained by Eq.(2). The instantaneous fluctuations were then used to obtain the root mean squared, r.m.s., of the turbulent fluctuation or the intensity of the turbulence.

$$\text{r.m.s.} = \sqrt{\overline{u_i'^2}} = \left\{ \frac{1}{N} \sum_{n=1}^{N} \left[u_i'^n(r, \theta, z, t) \right]^2 \right\}^{0.5} \tag{7}$$

As an example of the results from the first measurement (stagnant liquid case), Figure 8(a) shows the radial distribution of the mean velocity components, for the case when the bubble departed the viewing volume through Region I, closer to the wall. The velocity components were obtained by averaging the velocity vectors over the first time interval just after the bubble had left the viewing volume, i.e., from 0.133 s to 0.150 s on the time scale shown in Fig. 9. Figure 8(b) shows the Reynolds Stress distribution for the corresponding case.

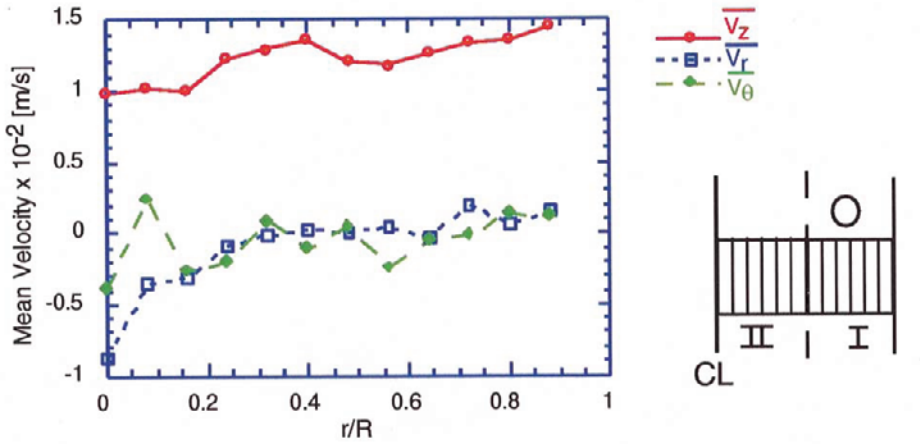

Fig. 8(a). Radial distribution of the mean velocity. Stagnant flow case.

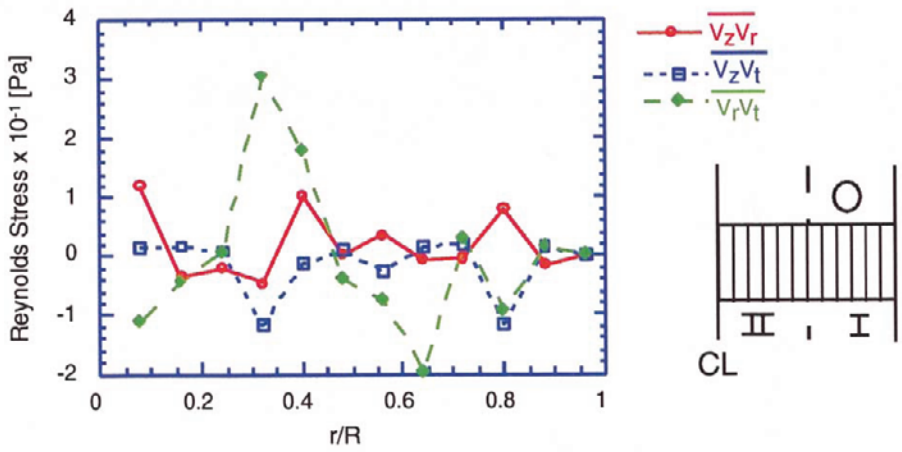

Fig. 8(b). Radial distribution of the reynolds stresses. Stagnant flow case.

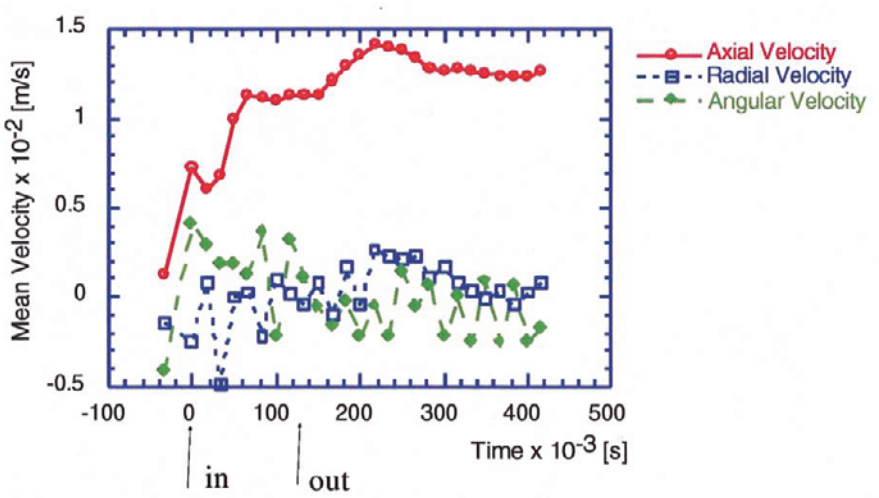

Fig. 9(a). Mean velocity components in the viewing volume. Stagnant flow case.

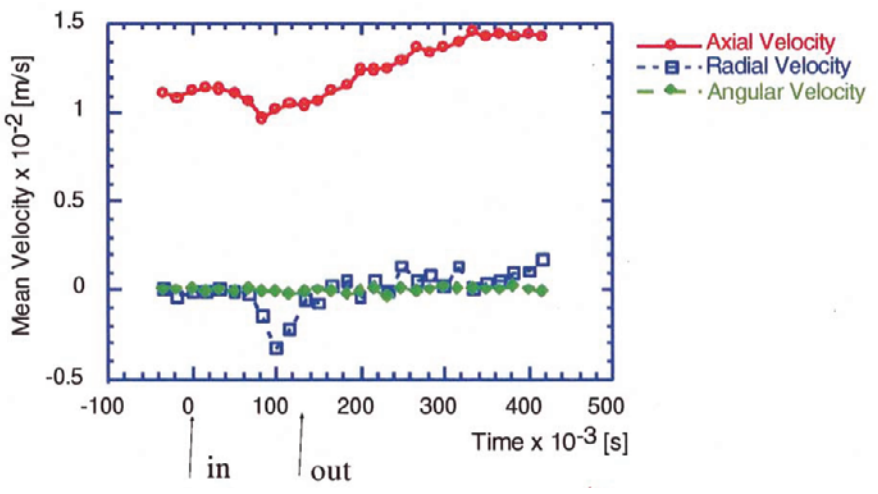

Fig. 9(b). Mean velocity components in the viewing volume. Co-current flow case.

Figure 9(a) shows the mean value of each velocity component as a function of time. The fluid was stationary prior to the arrival of the bubble to the test section. In this figure, time zero refers to the instant when the bubble first appears in the viewing volume. The bubble departed the viewing section at 0.133 s. Figure 9(b) illustrates the mean velocity components behavior for the upward concurrent flow.

The kinetic energy values are shown in Fig. 10. The mass of the liquid has been set to a value of one. The data points for these energy plots were calculated by using an ensemble average over the whole viewing volume for each period of time. For the first measurement, Figure 10(a), it is clearly shown that once the bubble reaches the viewing region, it generates a high turbulent motion in the fluid. The mean kinetic energy of the fluid is very small. After the bubble leaves the viewing volume (0.133 s), it generates a wake. At ~0.070 s after the bubble leaves the viewing section, the effect of the wake is diminishing, consequently; the turbulent kinetic energy starts reducing, as also noted by Song et al. (1996). Figure 10(b) shows the behavior for the co-current flow case.

The transient behavior of the kinetic energy for the co-current flow case does not show a sharp rise in the kinetic energy at time zero, as occurred for the stationary fluid case. Moreover, the turbulent kinetic energy is smaller compared with the previous case. Also it should be noted that the decay in the energy is delayed until ~0.270 s after the bubble departure from the viewing volume, as is also observed by Song et al. (1996).

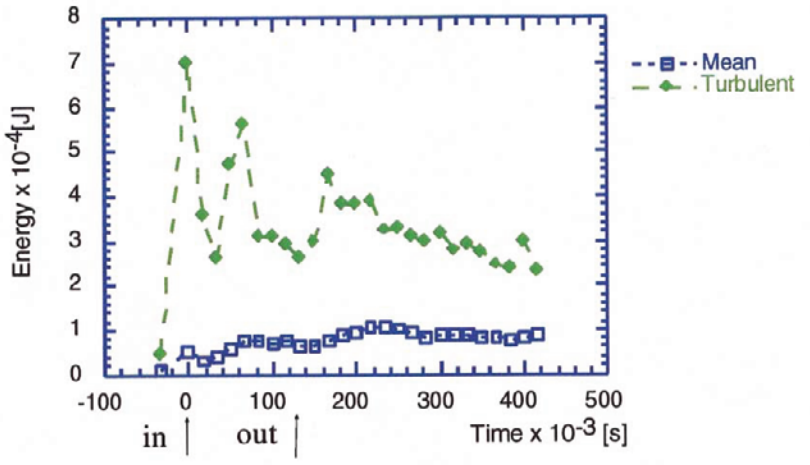

Fig. 10(a). Turbulent kinetic energy and mean kinetic energy in the viewing volume. Stagnant flow case.

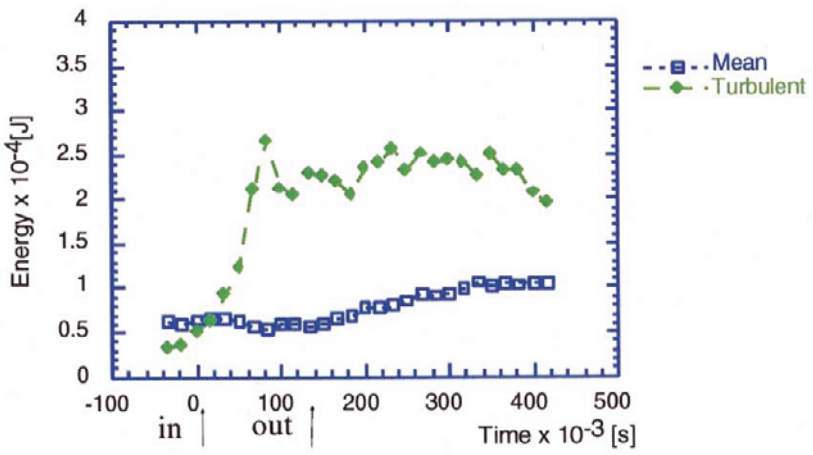

Fig. 10(b). Turbulent kinetic energy and mean kinetic energy in the viewing volume. Co-current flow case.

6. Conclusions

The PIV technique has been extended to study three-dimensional two-phase flows. It has demonstrated its ability to provide quantitative velocity information in such a manner that several advantages can be realized over the more traditional methods. Different two-phase situations have been presented and the instantaneous full-field velocity fields for fluid phases are measured. PIV is a promising powerful tool to study the structure of multiphase flows.

References

Adrian, R. J., Particle-Imaging Techniques for Experimental Fluid Mechanics, Annu. Rev. of Fluid Mech., Vol. 23 (1991), 261-304.

Adrian, R. J., Multi-point Optical Measurements of Simultaneous Vectors in Unsteady Flow- A review, Int. J. Heat Transfer Fluid Flow, Vol. 7 (1986), 127.

Cenedese, A., Romano, G.P., Paglialunga, A. and Terlizzi, M., Neural Net for trajectories recognition in a flow, Sixth Int. Sy mp. on Applications of Laser Techniques to Fluid Mechanics, Lisbon, Portugal, (1992), 27.1.1-27.1.6.

Chinnov, E. A. and Volkov, P. K., Bubble Motion in Vertical Channels, Phase Interface Phenomenon in Multiphase Flow, (1991), 231-243.

Costes, S. V., Development of a Three-Dimensional Particle Image Velocimetry Algorithm and Analysis of Synthetic and Experiment al Flows in Three-dimensions, (1994), Thesis, Texas A&M University.

Gonzalez, R. C. and Wintz, P., Digital Image Processing, (1987) Addison-Wesley Publishing Company, Inc., Reading, Massachusetts.

Grant, I. and Pan, X., An Investigation of the Performance of Multi Layer, Neural Networks Applied to the Analysis of PIV Image s, Experiments in Fluids, Vol. 19 (1995), 159-166.

Hassan, Y. A. and Philip, O., A New Artificial Neural Network Tracking Technique For Particle Image Velocimetry, Experiments in Fluids, Vol. 22.

Hassan, Y. A. and Blanchat, T., Measurement of Two-Phase Interfacial Drag in Stratified Flow with Pulsed Laser Velocimetry, In Imaging in Transport Processes, (1993), 283-294, Begell House, Inc., New York.

Hassan, Y. A., Blanchat T. K. and Seeley Jr., C. H., PIV Flow Visualization Using Particle Tracking Techniques, Measurements in Science and Technology, Vol. 3 (1992a). 633-642.

Hassan, Y. A., Blanchat, T. and Seeley Jr., C. H., Simultaneous Velocity Measurements of Both Components of a Two-Phase Flow us ing Particle Image Velocimetry, Int. Journal of Multiphase Flow, Vol. 18, No. 3 (1992b), 71-395.

Hilgers, St. and Merzkirch, W., Particle Velocity and Particle Concentration in a Three-Phase Flow, Proceedings of the Sixth In ternational Symposium on Applications of Laser Techniques to Fluid Mechanics and Workshop on Computers in Flow Measurements, July 20-23, (1992), 9.1.1-9.1.4.

Kasagi, N. and Nishino, K., Probing Turbulence with Three-Dimensional Particle-Tracking Velocimetry, Experimental Thermal and F luid Science, Vol. 4 (1991), 601-612.

Moursali, E., Marie, J. L. and Bataille, J., An Upward Turbulent Bubbly Boundary Layer Along a Vertical Flat Plate, Int. J. Mul tiphase Flow, Vol. 21, No. 1(1995), 107-117.

Murai, Y. and Matsumoto, Y., Three Dimensional Structure of a Bubble Plume: Measurement of the Three Dimensional Velocity, FED- Vol. 209, Flow Visualization and Image Processing of Multiphase Flow Systems, Proceedings of the 1995 ASME/JSME Fluids Engineering and La ser Anenometry Conference and Exhibition, August 13-18, 1995.

Nishino, K., Kasagi, N. and Hirata, M., Three-Dimensional Particle Tracking Velocimetry Based on Automated Digital Image Processing, Journal of Fluids Engineering, Vol. 111(1989), 384.

Oakley, T. R., Loth, E. and Adrian, R. J., Cinematic Two-Phase PIV for Bubbly Flow, FED-Vol. 209, Flow Visualization and Image Processing of Multiphase Flow Systems, Proceedings of the 1995 ASME/JSME Fluids Engineering and Laser Anenometry Conference and Exhibition, August 13-18, 1995, (1995), 123-130.

Okamoto, K., Schmidl, W. and Hassan, Y. A., New Tracking Algorithm for Particle Image Velocimetry, Experiments in Fluids , Vol. 19 (1995), 342-347.

Philip, O., Schmidl, W. and Hassan, Y. A., Development of a High Speed Particle Image Velocimetry Technique Using Fluorescent T racers to Study Steam Bubble Collapse, Nuclear Engineering and Design, Vol. 149 (1994), 375-385.

Reese, J., Chen, R. C. and Fan, L. S., Three-dimensional Particle Image Velocimetry for use in Three-Phase Fluidization Systems , Experiments in Fluids, Vol. 19 (1995), 367-378.

Song, X., Yamamoto, F., Iguchi, M., Koketsu, M. and Chen, G., 3-D PTV Measurement of Bubble Rising Flow in a Cylindrical Vessel , ISIJ International, Vol. 36, Supplement (1996), S54-S57.

Sridhar, G. and Katz, J., Drag and Lift Forces on Microscopic Bubbles Entrained by a Vortex, Phys. Fluids, Vol. 7, No. 2 (1995), 389-399.

Trigui, N., Guzennee, Y., Brodkey, R. and Kent, C, Algorithms for Fully Automatic Three-Dimentional Particle Image Velocimetry, Proceeding of the Thirteenth Symposium on Turbulence, Sept. 1992, Rolla, Missouri, (1992) B27.

Yamamoto, F., Iguchi, M., Ohta, J. and Koketsu, M., Measurement of Bubbling Two-Phase Flow Using 3-D PTV Based on Binary Image Cross-Correlation Method, FED-Vol. 209, Flow Visualization and Image Processing of Multiphase Flow Systems, Proceedings of the 1995 ASME/JSME Fluids Engineering and Laser Anenometry Conference and Exhibition, August 13-18, (1995a), 131-136.

Yamamoto, F., Iguchi, M., Wada, A. and Koketsu, M., Mathematical Fundementals of the Binary Image Cross-Correlation Method for 2-D and 3-D PTV, Proceedings of the International Workshop on PIV- Fukui '95, Jul 2-5, (1995b), 79-90.

Authors' Profiles

Yassin A. Hassan : He (BS, nuclear engineering, University of Alexandria, 1968 ; Ms, 1975, and Ph. D., 1979, nuclear engineering, University of Illinois ; MS, mechanical engineering, University of Virginia, 1985) is a professor and graduate coordinator in the Department of Nuclear Engineering at Texas A&M University. His interests include computational and experimental fluid flow, turbulence, two-phase flows, laser velocimetry and imaging techniques, and nuclear reactor safety.

William Daniel Schmidl : He received his BS(Eng) degree in marine systems engineering in 1990 from the United States Merchant Marine Academy and his M.S degree in nuclear engineering in1992 from Texas A&M University. His research interests are in the area of experimental fluid flow and quantitative full-field flow visualization using particle image velocimetry.

Javier Ortiz-Villafuerte : He is a Ph. D. candidate in Nuclear Engineering at Texas A&M University. He received a BSc degree in Physics and Mathematics from Escuela Superior de F ísica y Matem áticas (ESFM), Instituto Polit écnico Nacional (IPN), México, in 1992, and a MSc degree in Nuclear Engineering from Departamento de Ingenier ía Nuclear, ESFM, IPN, in 1994. He worked at Comisi ón Nacional de Seguridad Nuclear y Salvaguardias, M éxico, doing simulation of severe accidents for the Laguna Verde Nuclear Power Plant. His research areas are the application of computer vision techniques to flow visualization, and the development of neural networks as tracking algorithms in the study of two-phase flows.